

Ultrathin crystalline silicon solar cells by textured triangular grating

Xiaodong Lu¹ · Peng Zhang¹ · Yang Zhao¹ · Zelai Wang¹ ·
Yuanqing Wu¹ · Tao Zhou¹ · Hang Lv¹

Received: 21 June 2015 / Accepted: 12 October 2015 / Published online: 19 December 2015
© Springer Science+Business Media New York 2015

Abstract Grating structures can effectively enhance the light absorption abilities of solar cells with ultrathin active layer. In this work, a light trapping scheme composed of front surface triangular grating structure, bilayer antireflection coating and Ag back reflector is first designed for a ultrathin c-Si solar cell with a active layer thickness of 12 μm . The geometrical parameters of grating structure are then optimized by a dimensionless absorption enhancement factor. Finally, four methods are adopted to comprehensively evaluate the performances of the optimal grating structure, i.e. the front surface reflectance of external and internal light with different incident angles, intensity distribution of internal diffraction light and photocurrent density. The results show that the reflectance of external light with the incident angle smaller than 45° can be decreased to a level less than 5 %; light absorbed incompletely in a single pass through the active layer can obtain a diffraction angle larger than 38° for TE mode and 50° for TM mode in the c-Si active layer; internal nonzero-order diffraction light reflected by Ag back reflector can achieve a reflectance larger than 80 % at the front surface; the cell photocurrent density can reach 35.12 mA/cm^2 .

Keywords Solar cell · Crystalline silicon · Grating

1 Introduction

Recently, ultrathin crystalline silicon solar cells (UT c-Si SCs) with active layer thicknesses from a few micrometers to a few tens of micrometers have received tremendous interest because they can dramatically reduce the consumption of c-Si material and lower the quality requirements of c-Si materials for fabricating c-Si SCs (Li et al. 2014).

✉ Xiaodong Lu
lxd2211@tom.com

¹ College of New Energy, Bohai University, Jinzhou 121000, Liaoning, China

However, the efficiencies of UT c-Si SCs are still limited by serious optical losses caused by their UT active layers (Petermann et al. 2012). In order to effectively reduce the optical losses, researchers have developed many effective light trapping schemes (Mallick et al. 2012; Cui et al. 2013). Among these schemes, grating structures (GSs) have received much attention for their light absorption capabilities exceeding Lambertian limit in some specific wavelength ranges (Yu et al. 2011).

Studies show that one or two dimensional (1D or 2D) dielectric and metallic GSs on the front or back surfaces of SCs could effectively enhance the light absorption of active layer (Rana and Chun 2011) and the enhanced absorption effects of 2D GSs are better than those of 1D GSs (Angelo et al. 2012). Because the addition of metallic GSs increases the electron and hole recombination at the surface of the metal, which often negate the enhanced absorption effects of metallic GSs (Gjessing et al. 2010) and 2D dielectric GSs are computationally expensive and very sensitive to the incident angles of light (Yu et al. 2011), 1D dielectric GSs are a good choice for UT c-Si SCs. Previously published results also show that GSs on both the front and back surfaces of c-Si SCs have a better enhanced absorption effects than those only on the front or back surfaces (Rana and Chun 2011; Angelo et al. 2012), but their fabrications often need more complex and expensive fabrication processes, so they are not cost-effective light trapping schemes (Dominguez et al. 2012). In contrast, GSs only on the front or back surface of SC, which can be easily realized on substrate or superstrate, are more simple, cost-effective and large-scale light trapping schemes. In addition, studies also show that the enhanced absorption effects of GSs only on the front surface are equivalent to those of GSs only on the back surface (Darin et al. 2011).

Due to the weak absorption properties of c-Si materials in the long wavelength range near their band gaps, the thicknesses of UT c-Si active layers are a key factor for determining the enhanced absorption effects and geometric and physical parameters of GSs. Generally, the active layer is thinner, the enhanced absorption effects of GSs are better, but the efficiency of SCs are lower (Tseng et al. 2012; Mallick et al. 2012). In our previous work, we have analyzed thoroughly the influence of light trapping units, i.e. antireflection coatings (ARCs) and back reflectors (BRs), on the light absorption properties of c-Si active layers with different thicknesses (Lu et al. 2013). One of the most important conclusions is that when the active layer thicknesses gradually increase from 0.1 to 200 μm , the light absorption efficiency of c-Si active layer will first increase rapidly and then increase slowly and the thickness transition region is in the range from 10 to 20 μm . By setting the c-Si active layer thickness to a general thickness of 12 μm in the transition region and using a front surface texture structure (FSTS) with a simpler rectangular grating profile, we have achieved a photocurrent density of 32.46 mA/cm^2 , which is close to the photocurrent density levels obtained by those UT c-Si SCs with thicker active layer thicknesses and more complex light trapping schemes (Angelo et al. 2012; Tseng et al. 2012; Mallick et al. 2012). Therefore, the thickness transition region is an ideal thickness range for designing high efficiency and low cost c-Si SCs.

In this work, we expand on our previous work to optimize and analyze the light trapping performances of 1D GS with triangular profile by the same numerical method as that used in our previous work (Lu et al. 2013). Pursuant to that, the active layer thickness of UT c-Si SC in this work is also chosen as 12 μm and the light trapping schemes include the basic light trapping units used in thick commercial c-Si SCs, i.e. ARCs and BRs. Generally, the most common methods to evaluate the performances of light trapping schemes are reflectance spectra, cell photocurrent density or dimensionless absorption enhancement factor (Angelo et al. 2012; Gjessing et al. 2010; Yu et al. 2011). In fact, the results obtained

by these methods are overall evaluations for the enhanced absorption effects of all light trapping units, including ARCs, GSs and BRs. Theoretically, the functions of GSs on cell's front surfaces include three aspects: decreasing the reflectance of external light incident on the front surface, changing the direction of the incident light into several diffraction directions and decreasing the leakage losses of internal light reflected back by BRs. Therefore, in addition to evaluating the overall performances of our light trapping scheme by photocurrent density, we will adopt some accurate methods for evaluating the light trapping performances of front surface GSs according to the propagation process of external light in UT c-Si SCs.

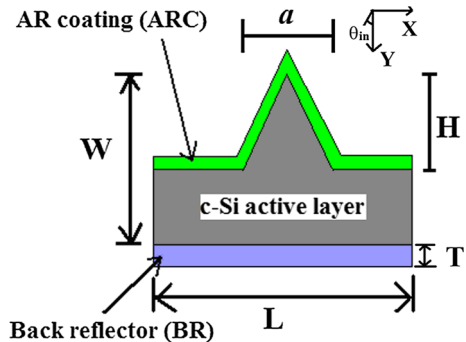
2 Cell structure and numerical methods

2.1 Cell structure

The c-Si SC structure under investigation is shown in Fig. 1, where 1D periodic triangular grating (TG) FSTS is fabricated on the front surface of c-Si active layer. In this work, the active layer thickness is indicated with W ($= 12\mu\text{m}$), the length, width and height of TG are represented by L , a and H , respectively and the thickness of BR is denoted by T . Filling factor f is defined as a/L and θ_{in} denotes the incident angle of light. The TG structure shown in Fig. 1 is frequently used in optoelectronic devices, such as semiconductor lasers and reflective optical filters, and it can be fabricated by standard micromachining process (Chen et al. 2010). In photo-voltage field, the TG structure is often realized by the following steps: the silicon wafer is first coated with a thin resist film and then the optimal TG pattern is fabricated onto the film by nanoimprint lithography (Xianqin et al. 2011; Yu et al. 2003) and holographic lithography (a maskless process) and finally an anisotropic etching process, such as reactive ion etching (RIE) technology is used to transfer the pattern on the film onto the silicon wafer.

In our simulation, a 200 nm thick Ag film is selected as BR, which can almost totally reflect light incident on its surface. Due to having better surface passivation properties and lower reflectivity, $\text{SiO}_2/\text{Si}_3\text{N}_4$ double layer is used as ARC, where the thicknesses of SiO_2 and Si_3N_4 layers are 94 nm and 67 nm, respectively. The reflectance spectra of TE- and TM-polarized light incident on the ARC are shown in Fig. 2, where the numerical method is transfer matrix method and no FSTS exists on the front surface of active layer. Figure 2a and b show that the reflectances of TE-polarized light with the θ_{in} range from 0° to 30° and

Fig. 1 A scheme of the UT c-Si SC patterned with a TG FSTS



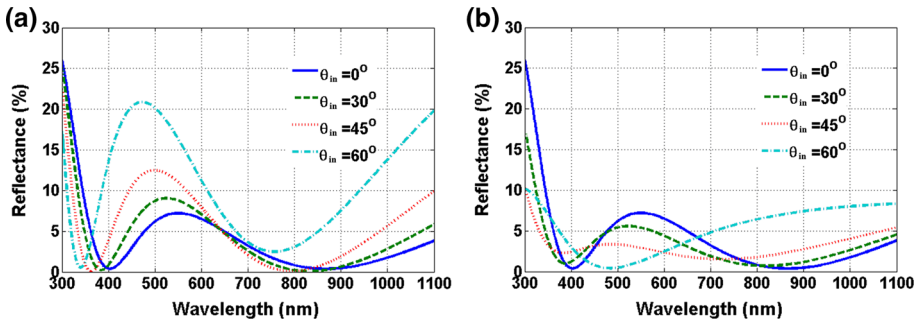


Fig. 2 The reflectance spectra of light incident on the ARC at different θ_{in} values, where **a** and **b** are the reflectance spectra of TE- and TM-polarized light, respectively. θ_{in} denotes the incident angle

TM-polarized light with the θ_{in} range from 0° to 60° are all lower than 10 % in the wavelength range from 350 to 1100 nm.

2.2 Numerical methods for optimizing grating geometrical parameters

Two dimensional finite-difference frequency-domain (FDFD) method, which is one of most rigorous numerical methods to deal with complex electromagnetic field problems, is used to optimize grating structures (Lu et al. 2013; Rumpf 2012). In the simulation process, we put two perfect matched layers (PML) on the top and bottom boundaries of computation area in the Y direction and set periodic boundary conditions (PBC) in the X direction. In order to effectively decay the evanescent fields and increase the computational accuracy, two spacer regions are added between the cell and PML layers. A plane wave source with unit amplitude is incident from the top boundary of our computation area and two record planes are set on the boundaries of two spacer region far away from the cell, respectively, to record the reflected and transmitted fields. In the post data process, the fraction of power in each diffracted order is first calculated by Fourier transforming the diffracted field amplitudes and the reflectance $R(\lambda)$ and transmittance $T(\lambda)$ are then obtained by summing the powers of reflected and transmitted field in all diffraction orders. The total absorptance $A_{total}(\lambda)$ of a c-Si SC at each wavelength for different light trapping schemes can be calculated by:

$$A_{total}(\lambda) = 1 - T(\lambda) - R(\lambda) \tag{1}$$

We assume that the absorption of incident light only exists in the active layer and Ag BR, so the effective absorptance A_{EFF} of a c-Si SC can be easily obtained by,

$$A_{EFF}(\lambda) = A_{total}(\lambda) - A_{BR}(\lambda) \tag{2}$$

where A_{BR} is the absorptance of light only in the BR.

The photocurrent density J_{ph} , which is usually used to evaluate the different mechanisms of light losses, can be represented by (Chen et al. 2010),

$$J_{ph} = \frac{q}{hc} \int_{\lambda} \lambda' A(\lambda') \frac{dI}{d\lambda'} d\lambda' \tag{3}$$

where q , h , c and λ are the charge on an electron charge, Planck’s constant, speed of light and wavelength, respectively; A is the corresponding absorptance of different mechanisms,

such as the absorption of light in active layer, BR or c-Si SCs with different light trapping schemes; $dI/d\lambda$ is the power density per unit wavelength of the solar radiation (ASTM AM1.5 Global tilt).

The optimal geometrical parameters for TG FSTs can be obtained by evaluating the values of dimensionless absorption enhancement factor EF , which is defined as (Lu et al. 2013),

$$EF = \frac{\frac{1}{\lambda_2 - \lambda_1} \int_{\lambda_1}^{\lambda_2} A_{EFF}(\lambda) d\lambda}{\frac{1}{\lambda_2 - \lambda_1} \int_{\lambda_1}^{\lambda_2} \alpha(\lambda) d\lambda} = \frac{\int_{\lambda_1}^{\lambda_2} A_{EFF}(\lambda) d\lambda}{\int_{\lambda_1}^{\lambda_2} A_{AL}(\lambda) d\lambda} \tag{4}$$

where $A_{EFF}(\lambda)$ is the effective light absorbance of a c-Si SC [as shown by Eq. (2)], $A_{AL}(\lambda)$ are the light absorbance of a SC only with active layer and without any light trapping schemes, and λ_1 and λ_2 are the two boundary wavelengths for a given wavelength range. The physical meaning of EF is the average absorption ratio between active layers with optimal light trapping scheme and without any light trapping schemes.

2.3 Numerical methods for evaluating the performance of TG FSTs

According to the propagation process of external incident light in the UT c-Si SC, the performances of FSTs can be evaluated by three methods: the front surface reflectance of external light with different incident angles incident on the front surface of a SC, the distribution of diffraction light inside solar cell and the front surface reflectance of internal

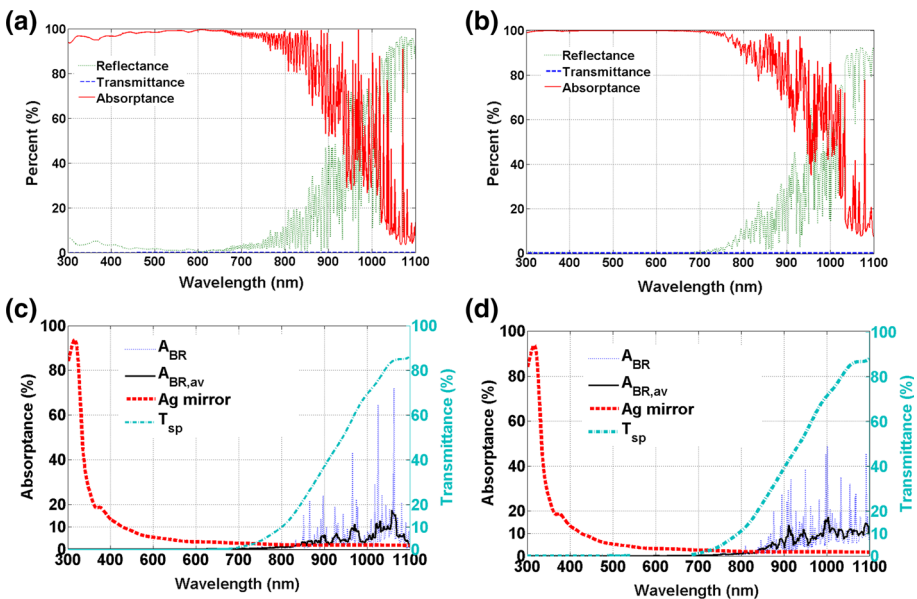


Fig. 3 The absorbance spectra of a c-Si SC and its Ag BR, where **a** and **b** are the total absorbance spectra of TE and TM polarized light calculated by Eq. (1), respectively and **c** and **d** are the absorbance spectra of TE and TM polarized light in Ag BR, respectively

light incident on the front surface of a SC. In this work, the performances of FSTs are evaluated by these methods and the comprehensive performances of SCs are evaluated by the effective photocurrent density.

The effect photocurrent density $J_{\text{ph,eff}}$ is defined as,

$$J_{\text{ph,eff}} = J_{\text{ph,act}} - (J_{\text{rad}} + J_{\text{SRH}} + J_{\text{Auger}}) \quad (5)$$

where $J_{\text{ph,act}} (= J_{\text{ph,total}}(\lambda) - J_{\text{ph,BR}}(\lambda))$ is the photocurrent density generated in active layer and J_{rad} , J_{SRH} and J_{Auger} are the radiation, SRH and Auger recombination current density, respectively.

2.4 Evaluating the photocurrent density losses of different mechanisms

The photocurrent density losses of a c-Si solar cell with ARC, TG FSTs and Ag BR can be divided into two parts, i.e. the absorption losses of light in Ag BR and the losses caused by different photocarrier recombination mechanisms, such as radiation, SRH and Auger recombination. According to Ref. (Brendel 2003), a suitable assumption is that $J_{\text{SRH}} = 0$ (where SRH denotes Shockley–Read–Hall recombination caused by impurities), which means that no SRH recombination occurs in the volume of c-Si material and in the surface of active layer; when a c-Si active layers with Lambertian light trapping scheme is in the thickness range from 1 to 10,000 μm , J_{Auger} and J_{rad} will be in the range from 0.95 to 1.4 mA/cm^2 and from 7×10^{-2} to 2×10^{-2} mA/cm^2 , respectively. In our simulation, the total current loss (i.e. $J_{\text{SRH}} + J_{\text{rad}} + J_{\text{Auger}}$) is assumed to be 1 mA/cm^2 .

The absorption losses of light in Ag BR are related with the polarization properties of incident light. Figure 3 shows the absorptance spectra of polarized light in a c-Si SC (shown in Fig. 1) and its Ag BR, where the ARC parameters are as same as those in Fig. 2 and other parameters are as following: $W = 12 \mu\text{m}$, $H = 1 \mu\text{m}$, $L = 850 \text{ nm}$, $T = 200 \text{ nm}$, $f = 0.8$ and $\theta_{\text{in}} = 0^\circ$. As shown by Fig. 3a and b, the total absorptance spectra of TE and TM polarized light are mainly influenced by the reflectance spectra of incident light; due to the resonant FP cavity effects of c-Si active layer, the absorptance spectra of TE and TM polarized light show obvious oscillation forms in the wavelength range from 700 to 1100 nm; TM polarized light in the wavelength range from 300 to 700 nm can be nearly completely absorbed by the cell. The total photocurrent densities of TE and TM polarized light calculated by Eq. (3) are 35.73 and 36.99 mA/cm^2 , respectively.

The method for evaluating the values of A_{BR} is as following: the absorptance of Ag BR is first calculated by assuming that the image part of refractive index for c-Si active layer is set to zero at each wavelength, then the transmittance of light in a single pass through the active layer is obtained by setting the bottom PML of computation area immediately below the bottom boundary of active layer and a record plane on the bottom boundary of active layer. The absorptance of Ag BR at each wavelength can be represented by,

$$A_{\text{BR}}(\lambda) = A_{\text{AgBR}}(\lambda) \times T_{\text{sp}}(\lambda) \quad (6)$$

where A_{AgBR} is the absorptance of Ag BR without light absorption in active layer and T_{sp} is the transmittance of light in a single pass through the active layer. Due to neglecting the absorption of active layer (equivalent to increasing the reflection times of Ag BR), the values of A_{BR} are slightly larger than the real absorptance values of Ag BR.

Figure 3c and d show the values of A_{BR} and T_{sp} varying with wavelength. In addition, the absorptance of Ag mirror in air (“Ag mirror” curves) and the average values of ten

neighboring A_{BR} data points (“ $A_{BR,av}$ ” curves) are also given in Fig. 3c and d. As shown in Fig. 3c and d, the cutoff wavelength, which is the longest wavelength of light completely absorbed in a single pass through the active layer, is about 700 nm; the average values of A_{BR} (i.e. $A_{BR,av}$) for TE polarized light are nearly less than 10 % in the whole absorption wavelength range and, those for TM polarized light are larger than 10 % due to existing surface plasmon polaritons(SPPs). The photocurrent density losses of A_{BR} for TE and TM polarized light, which can be obtained by Eq. (3), are 0.8269 and 1.2356 mA/cm², respectively. Base on the above analysis, we can obtain that the total losses of photocurrent densities for TE and TM polarized light are 1.8269 and 2.2356 mA/cm², respectively.

3 Simulation results

The main characteristics of photo-electric conversion in a c-Si SC shown in Fig. 3 also indicate that the wavelength range from 700 to 1100 nm is the key wavelength range for designing a optimal TG FSTS; although the losses of Ag BR for TM polarized light are larger than those for TE polarized light, the $J_{ph,eff}$ value for TM polarized light is still larger than that for TE polarized light. In addition, the diffraction properties of incident light vary with its polarization properties, so the optimal parameters of a TG FSTS are also different for TE and TM polarized light. In the following, we will use TM polarized light to

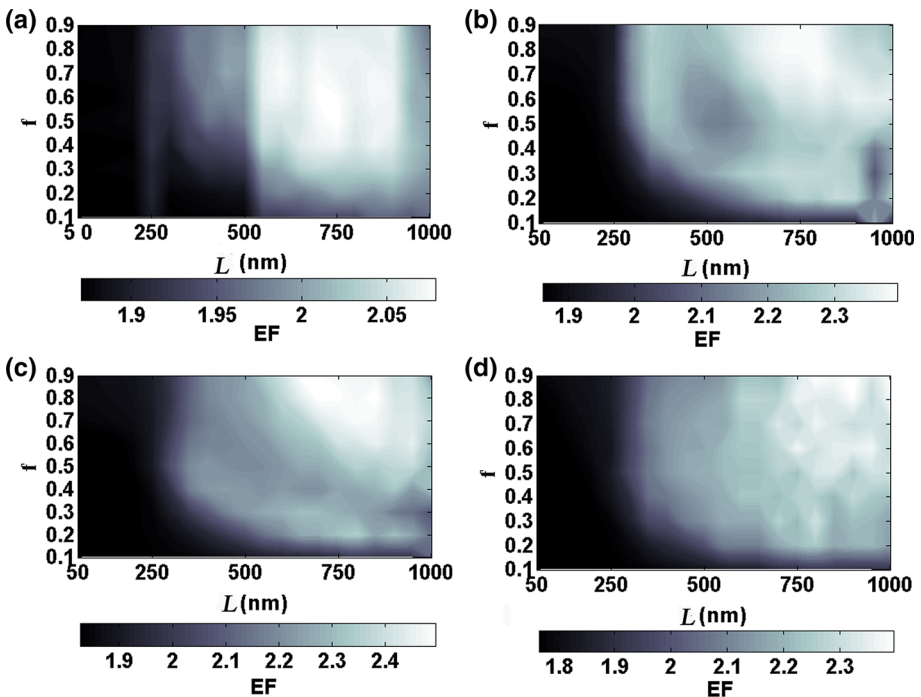


Fig. 4 The EF values varying with period length L , etching depth H and width of the high dielectric region a , where **a** $H = 50$ nm, **b** $H = 500$ nm, **c** $H = 1000$ nm and **d** $H = 2000$ nm, respectively. Different colors on the color bars represent different EF values

optimize the parameters of the TG FSTS shown in Fig. 1 and choose its total losses of photocurrent densities as 2.2356 mA/cm^2 for simplicity.

3.1 Optimizing the TG FSTS

Figure 4 shows that the EF values are related with period length L , etching depth H and filling factor f . In Fig. 4, the value of EF are calculated by,

$$EF = \frac{\int_{700}^{1100} A_{EFF}(\lambda) d\lambda}{\int_{700}^{1100} A_{AL}(\lambda) d\lambda} \quad (7)$$

where A_{EFF} is the effective absorbance of a c-Si SC with different parameters of TG FSTS and A_{AL} is the absorbance of active layer without any light trapping units. As shown in Fig. 4a–d, the maximum EF values mainly concentrate in the range of L from 600 to 800 nm and f from 0.5 to 0.9, and the minimum values of EF mainly concentrate in the range of L from 50 to 250 nm; with the etching depth H increasing gradually, the maximum value regions of EF will disappear gradually and appear at other regions with different values of L and f ; Table 1 gives the extreme values of EF in Fig. 4, where (H, L, f) values corresponding to the maximum EF values are (50 nm, 750 nm, 0.5), (500 nm, 750 nm, 0.9), (1000 nm, 850 nm, 0.8) and (2000 nm, 800 nm, 0.9), respectively. Here we choose the optimal parameters of our TG FSTS as $L = 850 \text{ nm}$, $f = 0.8$ and $H = 1000 \text{ nm}$, where $EF = 2.4940$.

3.2 Evaluating the performance of the TG FSTS

3.2.1 Reflection spectra of external incident light

The reflection spectra of external light incident on the front surface of our cell are shown in Fig. 5, where the bottom PML of computation area are set immediately below the bottom boundary of active layer, the active layer and bottom PML can completely absorb the incident light in a single pass and the reflection light recorded by the top record plane are only caused by the refractive index discontinuity in the upper surface of the SC. Figure 5a and b show that the reflectance of external incident light will increase with the θ_{in} values increasing from 0° to 75° for both TE- and TM-polarized light; in the wavelength range from 300 to 1100 nm, the reflectances of TE and TM polarized light with the θ_{in} values smaller than 45° are nearly lower than 5%. In contrast to Fig. 2, the TG FSTS of the cell can further decrease the reflectance of incident light with the θ_{in} value smaller than 45° and increase dramatically the absorption of light with a larger θ_{in} value; the acceptance capabilities of the cell for TE-polarized light have been notably enhanced; the light absorbance of the cell is not sensitive to the θ_{in} values in the range from 0° to 45° .

Table 1 The extreme values of EF in Fig. 4

| | $H = 50 \text{ nm}$ | $H = 500 \text{ nm}$ | $H = 1000 \text{ nm}$ | $H = 2000 \text{ nm}$ |
|-----------------------|---------------------|----------------------|-----------------------|-----------------------|
| Maximum value of EF | 2.0815 | 2.4685 | 2.4940 | 2.4658 |
| Minimum value of EF | 1.8528 | 1.8445 | 1.8155 | 1.7540 |

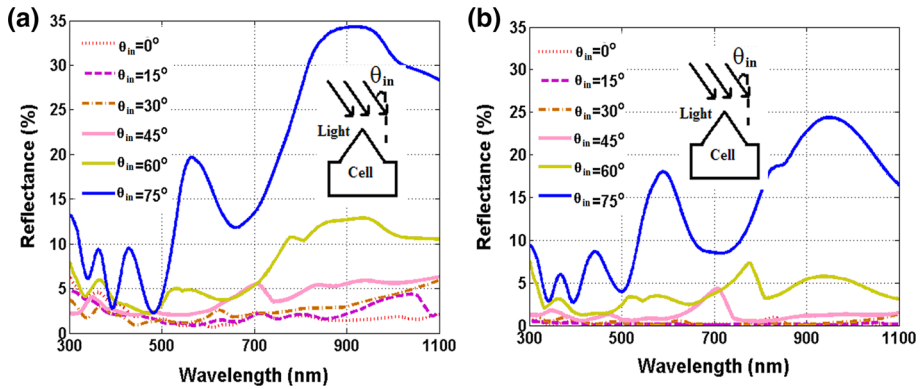


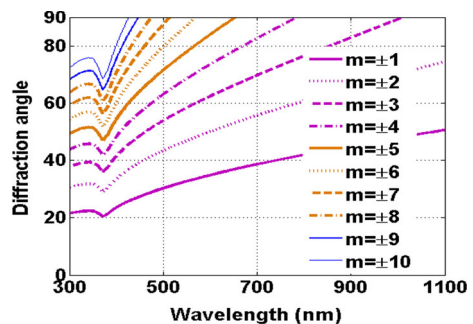
Fig. 5 The reflection spectra of external light incident on the front surface of our cell. **a** and **b** are TE- and TM-polarized light, respectively

3.2.2 Intensity distribution of diffraction light inside active layer

After external light incident on the front surface passes through the interface between ARC and active layer, it will exist in a form of diffraction light in the cell interior. For a given wavelength, the higher-order diffraction light will have a larger diffraction angle and correspond with a larger reflection angle of light reflected by Ag BR. Because the c-Si active layer thickness of our cell is equal to 12 μm , which has a 700 nm single-pass absorption cutoff wavelength, here we only consider light in the wavelength range from 700 to 1100 nm.

By assuming the image part of refractive index in c-Si active layer to be zero, a record plane setting on the bottom boundary of the active layer can record the diffracted field amplitudes of incident light passing through TG FSTS. The fraction of power in each diffracted order is calculated by Fourier transforming the diffracted field amplitudes and the diffraction angles can be obtained by the relation between diffracted order, transverse wave vector components and incident wave vector. Figure 6 gives the relationship between diffraction orders and diffraction angles, where external light is normally incident on our cell front surface. Figure 6 shows that smaller wavelengths have more diffraction orders; the diffraction angles of the same diffraction order will increase with wavelength increasing; external light with wavelength in the range from 700 to 1000 nm and from

Fig. 6 The relationships between diffraction order and diffraction angle at each wavelength, where m denotes the order number of diffraction light



1000 to 1100 nm have seven (i.e. $m = 0, \pm 1, \pm 2, \pm 3$) and five (i.e. $m = 0, \pm 1, \pm 2$) diffraction orders inside our cell, respectively. Figure 7 shows the light intensity distributions of different diffraction orders. As shown in Fig. 7, in the wavelength from 700 to 1100 nm, the light intensity of TE-polarized light mainly distributes in the first diffraction order (i.e. $m = \pm 1$) and that of TM-polarized light mainly distributes in the zero and second diffraction order (i.e. $m = 0$ and $m = \pm 2$). According to Fig. 6, the diffractive angles of TE-polarized light with wavelength in range from 700 to 1100 nm are larger than 38° and those of TM-polarized light in the same wavelength range are larger than 50° for nonzero order diffraction light.

3.2.3 Reflection spectra of internal incident light

Figure 8 is the reflection spectra of light incident from the bottom boundaries of active layer on the TG FSTS, which denotes the internal light reflected by Ag BR. Here we have assumed that no light losses exist in c-Si active layer and light will be completely absorbed by the top and bottom PMLs in a single pass. According to Figs. 6 and 7, the minimum diffractive angles of the nonzero order TE- and TM-polarized diffractive light in the wavelength range from 700 to 1100 nm are larger than 38° . As shown by Fig. 8a and b, this part of internal light can achieve a reflectance larger than 60 %. Zero-order diffraction light only exists in the diffraction order of TM-polarized light in the wavelength range from 700 nm to 1000 nm, and this part light, which accounts for about 50 % of the total light intensity (as shown in Fig. 8b), can obtain an average reflectance of about 40 %. Figure 8 shows that our cell front surface of can offer a good restriction for light reflected back from Ag BR.

3.2.4 Photocurrent density

Figure 9 gives the effective photocurrent density spectra of the c-Si cell, where external light is normally incident and the range of integrating wavelength is 1 nm. As shown by the cure of J3 in Fig. 9, our light trapping scheme can nearly completely absorb the light in the single-pass absorption wavelength range of the active layer with thickness of $12\mu\text{m}$ (i.e. 300–700 nm) and have good enhanced absorption effects in the wavelength range from 700 to 1100 nm. Figure 9 also shows that the total photocurrent density J3 of our cell can

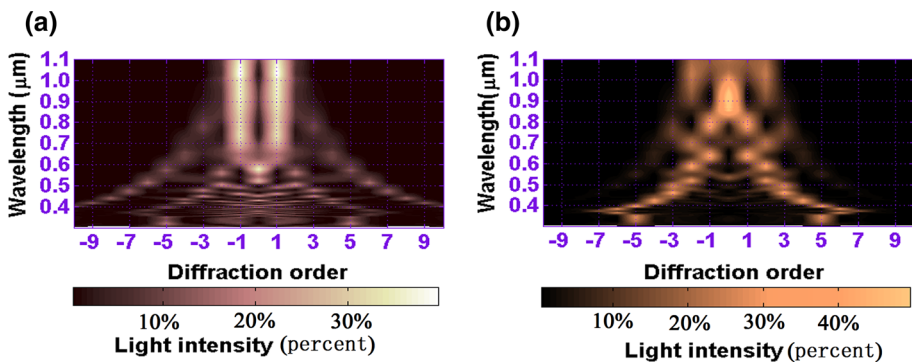


Fig. 7 The intensity distributions of light with different wavelengths at different diffraction orders, where **a** and **b** are the intensity distributions of TE- and TM-polarized light, respectively

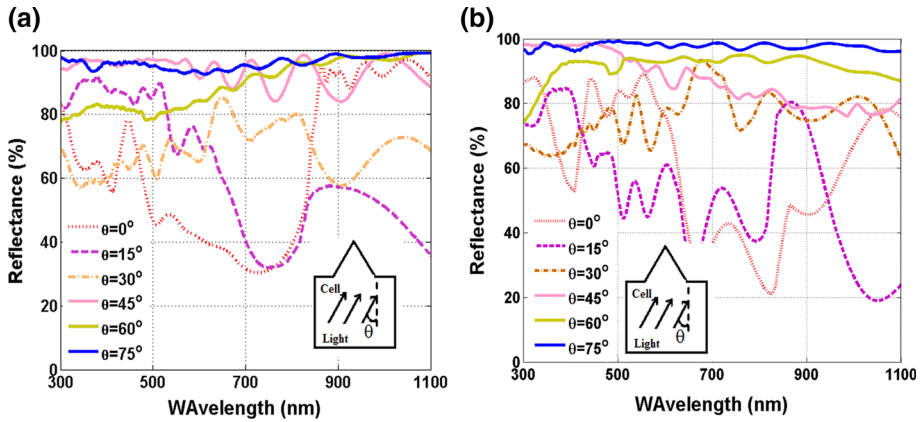


Fig. 8 The reflection spectra of internal light incident on the TG FSTS, where **a** and **b** are TE- and TM-polarized light, respectively

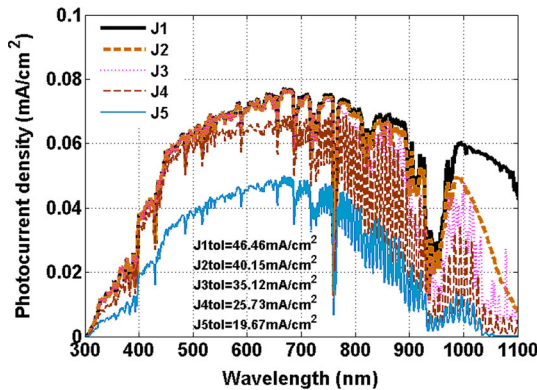


Fig. 9 The effective photocurrent densities of the c-Si SC under the AM1.5 spectrum, where J1 is the maximum possible photocurrent density of c-Si materials and J2, J3, J4 and J5 are the effective photocurrent densities of a 12 μm thick c-Si active layer with Lambertian light trapping schemes, our light trapping scheme, our light trapping scheme without TG FSTS and no light trapping schemes, respectively. J1 to 1, J2 to 1, J3 to 1, J4 to 1 and J5 to 1 are the totally effective photocurrent densities of J1, J2, J3, J4 and J5, respectively

reach 35.12 mA/cm^2 , which is close to the total photocurrent density J2 (40.15 mA/cm^2) of Lambertian light trapping scheme (J2 is an ideal theoretical value, where the reflection of external light incident on the front surface of c-Si SC has been neglected) and larger than the total photocurrent density J4 (25.73 mA/cm^2) of 12 μm flat active layer only with the ARC and BR and the total photocurrent density J5 (19.67 mA/cm^2) of 12 μm flat active layer without any light trapping units.

Our optimal light trapping scheme can enhance the light absorption of external incident light in the whole absorption wavelength range, as shown by Figs. 5, 6, 7 and 8, but due to the weak absorption properties of c-Si material in wavelength range near its band gap, the photogenerated current density in the wavelength range is still much lower than the maximum possible photocurrent density J1 in the same wavelength range. In order to

increase the light absorption in the wavelength range, researches have proposed various light trapping schemes for UT c-Si SCs. For example, Mutitu et al. designed a 5 μm thick c-Si SC with a photocurrent density of 30.3 mA/cm^2 by using a light trapping scheme with a binary grating FSTS with ARC and a dielectric Bragg grating BR (Mutitu et al. 2008); Chutinan et al. designed a 10 μm thick c-Si SC with a photocurrent density of 33.6 mA/cm^2 by using a light trapping schemes with single layer ARC, 2D photonic crystal FSTS and 1D triangular profile photonic crystal BR (Chutinan et al. 2009); Gjessing et al. (Gjessing et al. 2010) designed a 20 μm thick c-Si SC with a photocurrent density of 35.5 mA/cm^2 by using a light trapping scheme with single layer ARC, 2D photonic crystal back surface texture structure and Al BR; Lu et al. (Lu et al. 2013) designed a 12 μm thick c-Si SC with a photocurrent density of 32.45 mA/cm^2 by using a light trapping scheme with ARC, 1D photonic crystal FSTS and Ag BR. Compared with these results, although our cell can not absorb completely the light in the wave length range, it has achieved the highest light absorption efficiency by a comparatively simple light trapping scheme.

4 Conclusion

In this work, we have designed and optimized an effective light trapping scheme of TG FSTS for the UT c-Si SC with the active layer thickness of 12 μm . In order to comprehensively evaluate the light trapping performance of TG FSTS, some new evaluation method, including the reflectance of external and internal light and the intensity distribution of diffractive light inside the cell have been adopted in addition to the photocurrent density. Results show that our light trapping scheme can effectively enhance the light absorption ability of UT c-Si active layer and its photocurrent density is very close to that of Lambertian light trapping scheme.

Acknowledgments This work was supported by program for Educational commission of Liaoning province of China (No: L2012401) and National Science Foundation for Distinguished Young Scholars of China (No:11304020).

References

- Angelo, B., Marco, L., Lucio, C.A.: Photonic light-trapping versus lambertian limits in thin film silicon solar cells with 1D and 2D periodic patterns. *Opt. Express* **20**(S2), A224–A244 (2012)
- Brendel, R.: *Thin-film Crystalline Silicon Solar Cells Physics and Technology*. WILEY-VCH Verlag GmbH & Co. KGaA, Weinheim (2003)
- Chen, C., Niels, V., Kristof, L., et al.: Groove-gratings to optimize the electric field enhancement in a plasmonic nanoslit-cavity[J]. *J. Appl. Phys.* **108**, 034319-1–034319-8 (2010)
- Chutinan, A., Kherani, N.P., Zukotynski, S.: High-efficiency photonic crystal solar cell architecture. *Opt. Express* **17**(11), 8871–8878 (2009)
- Cui, H., Pillai, S., Patrick, C., et al.: A novel silver nanoparticle assisted texture as broadband antireflection coating for solar cell applications. *Sol. Energy Mater. Sol. Cells* **109**, 233–239 (2013)
- Darin, M., Rahul, D., Dietmar, K.: Influence of front and back grating on light trapping in microcrystalline thin-film silicon solar cells. *Opt. Express* **19**(S2), A95–A107 (2011)
- Dominguez, S., Garcia, O., Ezquer, M., et al.: Optimization of 1D photonic crystals to minimize the reflectance of silicon solar cells. *Photon. Nanostructures Fundam. Appl.* **10**, 46–53 (2012)
- Gjessing, J., Marstein, E.S., Sudbø, A.: 2D back-side diffraction grating for improved light trapping in thin silicon solar cells. *Opt. Express* **18**(6), 5481–5495 (2010)

- Li, G., Li, H., Jacob, Y.L., et al.: Nanopyramid structure for ultrathin c-Si tandem solar cells. *Nano Lett.* **14**(5), 2563–2568 (2014)
- Lu, X., Lun, S., Zhou, T., et al.: A low-cost high-efficiency crystalline silicon solar cell based on one-dimensional photonic crystal front surface textures. *IOP J. Opt.* **15**(7), 075705-1–075705-10 (2013)
- Mallick, S.B., Agrawal, M., Wangperawong, A., et al.: Ultrathin crystalline-silicon solar cells with embedded photonic crystals. *Appl. Phys. Lett.* **100**(5), 053113-1–053113-3 (2012)
- Mutitu, J.G., Shi, S., Chen, C., et al.: Thin film silicon solar cell design based on photonic crystal and diffractive grating structures. *Opt. Express* **16**(9), 15238–15248 (2008)
- Petermann, J.H., Zielke, D., Schmidt, J., et al.: 19%-efficient and 43 μm -thick crystalline Si solar cell from layer transfer using porous silicon. *Prog. Photovolt. Res. Appl.* **20**(1), 1–5 (2012)
- Rana, B., Chun, X.: Nano-crystalline silicon solar cell architecture with absorption at the classical $4n^2$ limit. *Opt. Express* **19**(S4), A664–A672 (2011)
- Rumpf, R.C.: Simple implementation of arbitrarily shaped total-field/scattered-field regions in finite-difference frequency-domain. *Prog. Electromagn. Res. B* **36**(1), 221–248 (2012)
- Tseng, P.C., Tsai, M.A., Yu, P., et al.: Antireflection and light trapping of subwavelength surface structures formed by colloidal lithography on thin film solar cells. *Prog. Photovolt. Res. Appl.* **20**(2), 135–142 (2012)
- Xianqin, M., Guillaume, G., Ounsi, E.D., et al.: Absorbing photonic crystals for silicon thin-film solar cells: design, fabrication and experimental investigation. *Sol. Energy Mater. Sol. Cells* **95**(Supplement 1), S32–S38 (2011)
- Yu, Z., Gao, H., Wu, W., et al.: Fabrication of large area subwavelength antireflection structures on Si using trilayer resist nanoimprint lithography and liftoff[J]. *J. Vac. Sci. Technol. B* **21**(6), 2874–2877 (2003)
- Yu, Z., Raman, A., Fan, S.: Nanophotonic light-trapping theory for solar cells. *Appl. Phys. A* **105**(2), 329–339 (2011)